Ultrasonics 86 (2018) 14–19

Contents lists available at ScienceDirect

Ultrasonics

journal homepage: www.elsevier.com/locate/ultras

Ultrafast laser pulse chirp effects on laser-generated nanoacoustic strains in Silicon

M. Bakarezos [a,b,*], E. Tzianaki [c], S. Petrakis [a], G. Tsibidis [d], P.A. Loukakos [d], V. Dimitriou [a], C. Kosmidis [c], M. Tatarakis [a], N.A. Papadogiannis [a,b]

[a] Centre for Plasma Physics and Lasers, School of Applied Sciences, Technological Educational Institute of Crete, Tria Monastiria, 741 00 Rethymno, Greece
[b] Department of Music Technology & Acoustics Engineering, School of Applied Sciences, Technological Educational Institute of Crete, 1 E. Daskalaki Str., 741 33 Rethymno, Greece
[c] Physics Department, School of Sciences, University of Ioannina, 451 10 Ioannina, Greece
[d] Foundation for Research and Technology – Hellas (FORTH), Institute of Electronic Structure and Laser (IESL), N. Plastira 100, Vassilika Vouton, 700 13 Heraklion, Greece

ARTICLE INFO

Article history:
Received 14 September 2017
Received in revised form 20 December 2017
Accepted 16 January 2018
Available online 4 February 2018

Keywords:
Picosecond ultrasonics
Ultrafast acoustics
Laser ultrasonics
Nanoacoustic strains
Laser pulse chirp
Silicon

ABSTRACT

Nanoacoustic strains are generated in Silicon by chirped femtosecond laser pulses using thin Titanium films as transducers. We investigate the effect that the generating laser pulse chirp has on the amplitude of the induced strains, manifested as Brillouin oscillations observed in degenerate femtosecond pump-probe transient reflectivity measurements. The strain amplitude is larger when negatively chirped pulses are used, which is attributed to the more efficient conversion of laser pulse light into acoustic strain in the Titanium transducer. Our present studies clearly show that the dependence of the Brillouin amplitude and the lattice strain is a non-monotonous function of the laser chirp parameter. An optimum negative laser pulse chirp is found for which the strain amplitude is maximized. A detailed thermomechanical model satisfactorily supports the experimental findings. In such a way, it is possible to suppress or enhance the induced nanoacoustic strain amplitude, thus all-optically controlling it by at least a factor of two.

1. Introduction

The study of very high frequency acoustic waves at a microscopic and nanoscopic level is a particularly active field of research. While MHz ultrasonic wave techniques have been extensively applied to many imaging and non-destructive testing applications, the development of ultrafast lasers and related all-optical pump-probe techniques opened the way for the generation and study of acoustic waves as short as a few picoseconds and of a bandwidth typically 100 GHz, thus opening the way for new applications. These include the non-destructive measurement of thermal and elastic properties of composite materials [1–3], the high-resolution microscopic characterization of interfaces [4,5] the study of vibrational modes of nanoparticles and nanostructured materials [6–8] the measurement of the ultrasonic attenuation in glasses [9,10] and the study of biological materials [11,12].

In what is usually referred to as *picosecond ultrasonics* [13,14] or *ultrafast acoustics*, an ultrashort "pump" laser pulse interacts with a transducer material (usually metallic) and a longitudinal strain pulse is formed. The transducer's lattice dynamics are governed by micro- and nano-acoustic strain localization that is generated either thermally or non-thermally [15–17]. The spatial extend of the localization depends on the material's response to the ultrafast laser excitation and the structure of the solid target and can be of the order of few nanometers [18] up to few tens of nanometers. The generated strains are monitored with a time-delayed "probe" laser pulse usually measuring changes in reflectivity. Applying these techniques in the nanoscale, for example in layered [19,20] and structured [21,22] materials, acoustic (phonon) frequencies up to the THz range have been demonstrated, while the generation of giant acoustic strain pulses in layered systems has been also reported [18].

To really extend the application potential of very high frequency acoustic waves their all-optical control on ultrafast time scales is highly desirable. This has been investigated both theoretically [23] and experimentally by using shaped laser pulses, for example, double-pulse excitation [24] and four-pulse excitation schemes [25]. An exciting possibility is the all-optical control using ultrashort laser pulses whose spectral content is rearranged in time, i.e. chirped pulses. For example, it has been demonstrated that the introduction of chirp affects the direct coherent phonon

* Corresponding author at: Centre for Plasma Physics and Lasers, School of Applied Sciences, Technological Educational Institute of Crete, Tria Monastiria, 741 00 Rethymno, Greece.
E-mail address: bakarezos@staff.teicrete.gr (M. Bakarezos).

https://doi.org/10.1016/j.ultras.2018.01.008
0041-624X/

generation in semiconductors [26]. This field is relatively unexplored experimentally, while there are no works that deal with the effect of chirped laser pulses on thermomechanical nanostrains induced in semiconductors through metal thin film transducer coating.

In a previous work we have studied the laser-generated acoustic strains in Ti:Si and Ag:Si layered systems using a degenerate transient reflectivity technique [27]. By probing the Brillouin scattering of laser photons from the generated strain waves within Si, we have investigated the role of the transducer film characteristics (electron-phonon coupling factor, acoustical impedance, thickness). We have demonstrated that localized, giant acoustic strains are produced when a 25 nm Ti film is used as a transducer. More recently, we have reported in a Letter clear indication that negatively chirped femtosecond (fs) laser pulses are capable of inducing larger strain amplitudes than unchirped and positively chirped pulses [28]. Here, we extend our studies in order to provide with more data and increase the resolution in the connection between the lattice strain and the laser chirp values aiming to both determine optimum values for strain amplitude maximization and to explore the strain dynamic range that can be accessed by this method. These new data reveal a remarkable effect, i.e. a non-monotonous behavior. This is supported by additional theoretical calculations, using a modified thermomechanical model based on the combination of a revised two-temperature model (TTM) and elasticity theory, which verify the experimental findings and predict the behavior for larger absolute values of the chirp parameter where experimental data are still not available.

2. The experimental method

The samples used in this study were layered structures (see Fig. 1a) consisting of a 25 nm thick Ti film deposited on 0.5 mm thick Si (1 0 0) monocrystal substrates by unbalanced dc magnetron sputtering. The Ti film served the role of a transducer for the conversion of laser pulse energy into acoustic strain. Ti was the material of choice since it has high electron-phonon coupling strength, high compressive yield strength, and its acoustical impedance is very well matched to that of Si [27]. Therefore, it converts very efficiently the laser pulse energy into acoustic strain, and it transfers very efficiently the acoustic strain into the Si substrate. Furthermore, it allows for a part of the fs probe laser pulses to reach the Si crystal, thus allowing for probing the acoustic strain that propagates inside it.

For the generation and detection of acoustic strains a degenerate pump-probe transient reflectivity technique was developed, described in detail in Refs. [27,28]. Both pump (generation) and probe (detection) laser pulses were derived from a Ti:Sapphire-based amplifier laser system, capable of producing pulses with energy up to 2 mJ and time duration 35 fs (full-width at half-maximum – FWHM). The repetition rate was 1 kHz while the center wavelength of the laser pulses was ~795 nm. The pump pulses were focused normally to the sample surface using a spherical mirror to achieve a fluence of 13 ± 1 mJ/cm^2, which was below the ablation threshold of Ti and into the thermoelastic regime for Ti. The probe pulses were focused at an angle of ~40° relative to the pump pulses using a parabolic mirror. The probe focusing area was centered with respect to the pump focusing area and its size was ~4 times smaller, yielding a fluence ~20 times smaller than the pump fluence, thus avoiding any contribution of the probe pulses to the excitation dynamics.

The probe pulses were variably delayed with respect to the pump pulses with a minimum temporal delay step of 0.8 fs. A lock-in detection technique, incorporating a balanced photodiode, was used for the detection of reflectivity changes after excitation (i.e. differences in reflectivity in the presence and the absence of the pump pulses). The detection scheme was sensitive enough for reflectivity changes of the order of ~10^{-5} to be resolved. Specially developed software was used to simultaneously control the temporal delay and detection instruments, and for data recording.

A linear chirp was introduced to the laser pulses, i.e. the instantaneous frequency of the laser pulses varied linearly with time:

$$\omega_{inst}(t) \equiv \omega - \frac{d\varphi(t)}{dt} \quad (1)$$

where ω and $\varphi(t)$ are the laser pulse carrier angular frequency and temporal phase, respectively. A pulse whose instantaneous frequency increases (decreases) linearly with time is positively (negatively) chirped. It has to be mentioned that the introduction

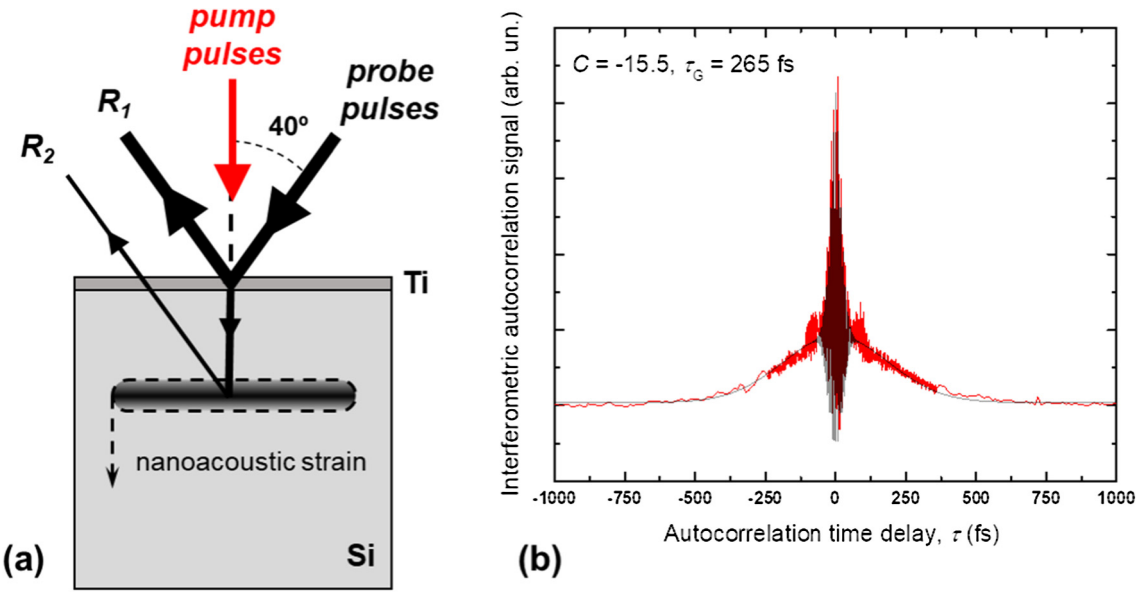

Fig. 1. (a) Schematic of the structure of the used samples and the principle of the detection scheme, (b) Typical experimental second-order interferometric autocorrelation signal (red line) and fit (grey line) using Eq. (3) (extracted parameters C and τ_G are also shown).

of such a chirp (positive or negative) in laser pulses results in the temporal broadening of the pulse. The chirp of the fs laser pulses was variably altered by changing the distance of the compressor gratings within the amplifier laser system. Fourier-transform-limited (FTL) laser pulses (35 fs time duration) were obtained for an optimal distance of the gratings, D_{opt}. Increasing this distance results in negatively chirped laser pulses, while positively chirped laser pulses are produced for distances smaller than D_{opt}. In order to know the time duration of the FTL and chirped pulses and to quantify the amount of the introduced chirp, second-order interferometric autocorrelations were performed using a commercially available system positioned just prior to the sample. Assuming a Gaussian profile, the electric field envelope of the linearly chirped laser pulses is given by [29]:

$$E(t) = E_0 e^{-(1+iC)\left(\sqrt{2\ln 2}\frac{t}{\tau_p}\right)^2} \tag{2}$$

where C is the chirp parameter ($C = 0$ for FTL pulses) and τ_p is the FWHM of the laser pulse temporal intensity profile. It must be mentioned that with the above definition the chirp parameter, C is negative (positive) for positively (negatively) chirped pulse. Both C and τ_p are extracted from the second-order interferometric autocorrelation data (e.g. see Fig. 1b), since for such laser pulses the interferometric autocorrelation, $G_2(\tau)$ can be determined analytically as [29]:

$$G_2(\tau) = 1 + 2e^{-\left(\frac{\tau}{\tau_G}\right)^2} + 4e^{-\left(\frac{C^2+3}{4}\right)\left(\frac{\tau}{\tau_G}\right)^2}\cos\left(\frac{C}{2}\frac{\tau^2}{\tau_G^2}\right)\cos(\omega\tau) + e^{-(1+C^2)\left(\frac{\tau}{\tau_G}\right)^2}\cos(2\omega\tau) \tag{3}$$

where τ is the time delay between the two pulses and $\tau_G = \tau_p/\sqrt{2\ln 2}$.

3. Results and analysis

Typical transient reflectivity results are shown in Fig. 2 for all different chirped laser pulses (data curves are vertically offset for clarity). These correspond to three cases of positively chirped pulses ($C = -13.5$, -15.5 and -20.0 with $\tau_G = 205$, 265 and 550 fs, respectively), three cases of negatively chirped pulses ($C = 6.5$, 16.0 and 21.0 with $\tau_G = 135$, 315 and 625 fs, respectively), and FTL pulses ($C = 0$ with $\tau_G = 30$ fs). At early times (pump-probe time delay ≤ 2 ps) an abrupt change in the reflectivity is observed for all cases (not shown in Fig. 2). This is related to the excitation and subsequent fast thermalization and cooling of the metal electrons: following laser excitation a portion of the initially excited non-thermal electrons thermalize through electron-electron and electron-phonon interactions. The reflectivity signal decays as thermal and non-thermal electrons transfer their excess energy to the lattice through electron-phonon interactions, diffusion, and ballistic transfer. After this electronic contribution, all the transient reflectivity signals exhibit sinusoidal-like oscillations superimposed onto a slow exponential decay. The period of these oscillations is ~13 ps, the same for all chirp cases. Furthermore, the amplitude of these oscillations decreases as the pump-probe time-delay decreases.

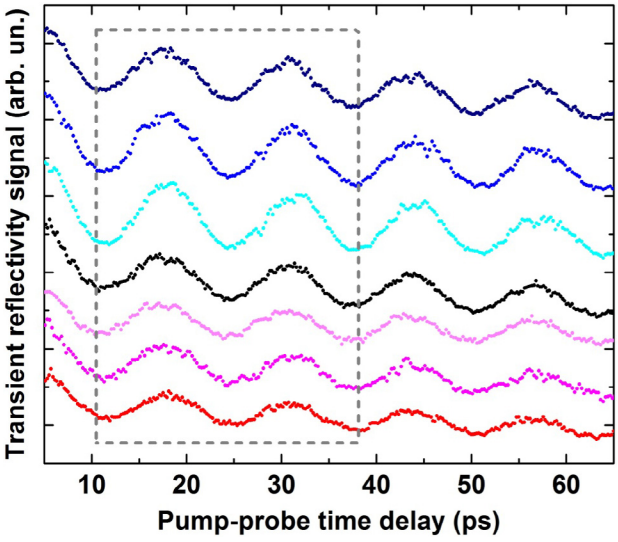

Fig. 2. Transient reflectivity signals vs. pump-probe time delay few picoseconds after the initial electronic contribution. The signals are displaced vertically for clarity. The value of laser chirp parameter, C, from top to bottom is 21.0, 16.0, 6.5, 0, −13.5, −15.5, and −20.0, respectively.

To understand the origin of these oscillations we need to elaborate on the detection scheme as illustrated in Fig. 1a. A substantial portion of the energy of the normally incident pump laser pulses is absorbed by the Ti film and is eventually converted into lattice movement. This results to the generation of a longitudinal nanoacoustic strain pulse in Ti which then enters the Si substrate and propagates inside it. Due to the very good acoustical impedance matching of Ti and Si the coupling efficiency of the strain into Si is very good [27]. The non-absorbed energy of the pump pulses is transmitted into Si as well; however, it is very small (typically ~15%) to cause any detectable excitation of Si.

A part of the probe pulses incident on the sample is reflected from it (R_1 in Fig. 1a). The Ti film is optically thin enough to allow for a small part of the probe pulses to be transmitted into Si. There the probe pulses meet the generated strain and again a part is reflected back towards the sample surface and eventually out of it (R_2 in Fig. 1a). The observed oscillations are due to the interference between the R_1 and R_2 pulses. In spite of the absorption and reflection losses at the interfaces (Si absorption is small at the probe wavelength and can be safely neglected) our detection system is sensitive enough to record the interference. The ~13 ps period of these oscillations corresponds to a 2π optical phase difference between the interfering beams. This prerequisites that the longitudinal acoustic strain has to travel a distance that corresponds to an optical delay of the probe beam ~2.7 fs, which is the probe beam E-field period, E_T. Maxima in the oscillations are observed when the optical time delay between the R_1 and R_2 pulses is an integer multiple of the E-field period (i.e. kE_T, where $k = 1, 2, 3\ldots$). Taking into account that the refractive index of Si at the probe wavelength, $n_{Si} = 3.7$, the optical path of the probe beam in Si is $d_{opt} = cE_T/n_{Si} \approx 219$ nm, where c is the speed of light in vacuum. The time required for the longitudinal acoustic strain to travel this distance is $\tau_{osc} = d_{opt}/2u_{Si} \approx 13$ ps, where u_{Si} is the longitudinal sound velocity in Si. Another way to understand the same phenomenon is to apply Bragg condition, so that the optical path difference between two successive maxima must be equal to the probe wavelength, λ (constructive interference between R_1 and R_2). Therefore:

$$d_{opt} = 2\tau_{osc}u_{Si} = \frac{cE_T}{n_{Si}} = \frac{\lambda}{n_{Si}} \Rightarrow \frac{1}{\tau_{osc}} = f_{Br} = \frac{2n_{Si}u_{Si}}{\lambda} \tag{4}$$

which is the well-known Brillouin scattering frequency (for normal incidence) observed when light experiences refractive index variations inside an optically transparent material due to lattice deformations. In our case, from Eq. (4) we calculate $f_{Br} \approx 80$ GHz corresponding to $\tau_{osc} \approx 13$ ps which exactly the oscillations period observed experimentally.

The interference origin (i.e. resulting from the interference between the R_1 and R_2 pulses shown in Fig. 1a) of these oscillations

is also the reason for the observed decrease of their amplitude as the pump-probe time delay increases [30] a situation similar to a field autocorrelation of two interfering beams. As is well known, the field autocorrelation trace of two temporally-delayed copies of a laser pulse measures the temporal coherence extend of the pulse, and the autocorrelation function of Gaussian-like laser pulses is also Gaussian-like with FWHM $\sim\sqrt{2}$ times broader than the FWHM of each pulse. For our case this means that a 50% decrease in the oscillations amplitude is expected for ~6 periods after the first observed oscillation maximum, in line with the experimental data presented here. Indeed, the expected acoustical damping up to the presented 100 ps pump-probe time delay (corresponding to ~850 nm acoustic strain travel distance inside Si) is estimated to be no more than 1% based on the acoustic attenuation data presented in Ref. [31]. Above that, it is worth noting that the optical absorption of the ~795 nm probe beam for the aforementioned acoustic strain travel distance inside Si is negligible and does not contribute to the decrease of the oscillations amplitude. The slow exponential decay the oscillations are superimposed on is attributed to the metal lattice temperature long temporal evolution [27] and its characteristic decay time is found to be 98 ± 5 ps, approximately the same for all chirp cases.

For a straightforward comparison of the oscillations amplitude in order to compare the effects of various laser pulse chirp cases on the acoustic strains in Si, we need to restrict in the pump-probe time delay range of ~10 ps to ~40 ps (region within the dotted line rectangular box in Fig. 2). The first Brillouin oscillation peak (observed at ~5 ps after excitation) must be excluded since it could be susceptible to influence from the metal electronic excitation and induced strains inside Ti alone. Given that the longitudinal sound wave velocity in Ti is ~6100 m/s, the time required for the generation and propagation of the induced strains so as to be well within Si, is ~5 ps. Furthermore, for pump-probe time delays greater than ~40 ps the decrease of the oscillations amplitude due to the interference origin of the oscillations cannot be safely neglected. Also note that to extract Brillouin amplitudes by means of sinusoidal-like fits to the experimental data, the slow exponential decay was first evaluated and then subtracted from all signals.

In Fig. 3, the extracted Brillouin oscillation amplitudes are shown for all laser pulse chirp cases. In Fig. 3 the computed peak strains are also shown, that have been calculated using a thermomechanical model based on the combination of a revised

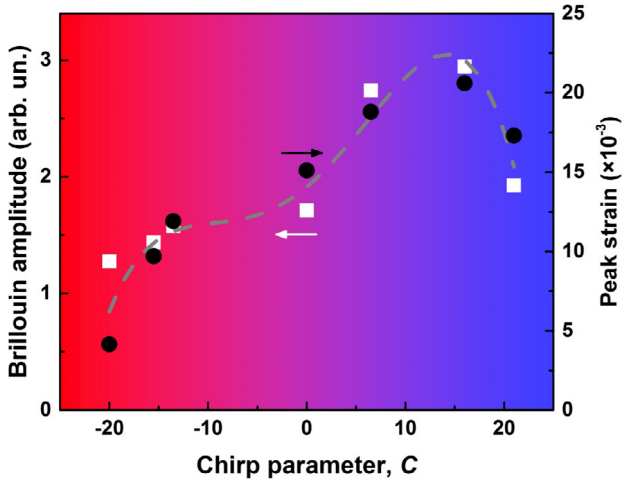

Fig. 3. Experimental Brillouin oscillation amplitudes extracted by sinusoidal fitting of the oscillations inside the grey parallelogram of Fig. 2 (white solid squares) and theoretically calculated peak acoustic strains (black solid circles) as a function of chirp parameter, *C*. The dashed grey line is a guide to the eye.

TTM [32–34] and elasticity theory, which has been successfully applied to our recent works [27,28]. This model accounts for the inclusion of non-thermal electron dynamics due to the ultrafast pulse duration, while also taking into account the instantaneous frequency changes of the chirped laser pulses.

Regarding modelling of the laser-matter interaction, it is known that the traditional TTM [35] assumes a rapidly (instantaneous) thermalization of the electronic distribution. Therefore, TTM yields an overestimation of the electronic temperature which has been also confirmed by pump-probe experiments [36]. To overcome the limitations of the TTM, analysis based on the Boltzmann's transport equations [37] or revised versions of the TTM [36,38–40] have been proposed. Those works presented the necessity for the inclusion of the initial non-thermal (NTH) electron population. More specifically, Sun at al. [40] used simultaneously a three-coupled equation-based model and Boltzmann's transport equation where heating of the electron gas by the initial NTH electrons and the lattice are included [40]. On the other hand, Lisowksi et al. proposed an improved version of the TTM by presenting a three-temperature model where a temperature for the NTH electrons was introduced [36]. Albeit these approaches successfully predicted results from pump-probe experiments for noble metals [40] or Ruthenium [36], they were characterized by the necessity of including fitting parameters [38]. Although it has been demonstrated that the most accurate model to describe the interaction of fs laser pulses with matter (including the contribution of the nonthermal electrons) is the one based on the Boltzmann's transport equations, its numerical complexity prevents exploitation of this approach for further analytical developments.

By contrast, in a recent approach presented by Carpene, an extension of the TTM was introduced by incorporating the electron thermalization dynamics into the source term, a potentially direct energy transfer from NTH electrons to the lattice and the consideration of a very-low-density NTH electron distribution [38]. The approach allows for a consistent calculation of the resulting (thermalized) electron temperature assuming the contribution of both the thermalized (TH) and NTH electron distributions. Validation of the model through pump-probe experiments illustrated that it provides an accurate description of ultrafast dynamics after irradiation of noble metals with ultrashort laser pulses [41–45]. In the present work, an extension has been performed to take into account not only the interaction of the nonthermal electrons with the electron and lattice systems (assuming also a relaxation time approximation of the nonthermal electron distribution [28]) but also a thermomechanical component was included to evaluate the role of the generation of strains.

It is evident that the electron-phonon coupling constant is a very important parameter towards evaluating the speed of the relaxation process and subsequent strength of the thermomechanical effects. The calculation of the coupling strength is based on the rate of the energy exchange between the electrons and the lattice which yields a dependence of the coupling constant on the electron temperature [46]. The electron-phonon coupling is calculated based on the above work in a self-consistent way: in other words, at every time step, the electron temperature value is used to compute the coupling strength that will be set in the next time step.

From the experimental data two major observations can be drawn: firstly, that negatively chirped pulses yield larger Brillouin oscillation amplitude compared to positively chirped or FTL pulses, and secondly that the Brillouin amplitude as well as the lattice strain exhibit a non-monotonous behavior with respect to the laser chirp parameter, *C*. This unavoidably leads to a value of *C* where the Brillouin amplitude is maximized, in spite the fact that the pulse duration is of the order of 200 fs. Further increase of *C* results in a decrease of the Brillouin oscillation amplitude. Such a behavior was not observed in our previous work [28],

and can be brought about only by the increased resolution in the laser chirp parameter in the experiments performed in the present work, thus providing with new data that elaborate on the effect that was initially observed in Ref. [28], i.e. that the lattice strain was constantly increasing (monotonous behavior) with increasing C (at least for the range of C values that were used there). This behavior is due to the way that the laser pulse interacts with the Ti transducer. In spite the fact that the electron temperature of the Ti transducer is maximum when FTL laser pulses are used, the final electron-lattice equilibrium temperature is higher for the case of negatively chirped pulses compared to both the cases of FTL and positively chirped pulses. This happens because when negatively chirped pulses are used, the temporally trailing edge of the pulse (less energetic photons) experiences new absorption channels in the energy region below the Fermi level that are created by the more energetic photons of the leading edge of the pulse. Thus, a relatively high number of nonthermal electrons is excited in higher energy states, leaving behind a higher number of empty states available for occupation deep below the Fermi level, leading to the new absorption channels of the less energetic photons which arrive later. On the other hand, this is not the case when positively chirped pulses are used, since the less energetic photons that initially interact with the Ti transducer are not able to open similar absorption channels deep enough for the more energetic photons to be efficiently absorbed. For the case of FTL laser pulses the electron temperature varies very quickly to the equilibrium temperature, thus the lattice bath that has high inertia cannot reach as high temperatures as for the case of negatively chirped pulses [28]. Of similar origin is the experimentally observed increase of the second harmonic signal from Au surface when negatively laser pulses are used rather than FTL or positively chirped pulses [47]. Our full study, where Ti was used as a transducer, shows that the Brillouin amplitude as well as the lattice strain maximizes in the range where $C = 16$. Although the introduction of negative chirp favors the conversion of laser optical energy into nanoacoustic strain, the resulting temporal broadening of the laser pulse tends to reduce the induced strains due to the lowering of the excitation laser intensity. Indeed, if the introduced laser pulse chirp exceeds this range ($C > 16$) the laser pulse intensity reduces significantly which leads to the observed reduction of the observed Brillouin oscillations amplitude.

The experimental results are fully supported by our theoretical model which incorporates the above laser pulse chirp effects. Indeed, as shown in Fig. 3 the computed peak strains (the value of which is indicative of the interference amplitude of the Brillouin oscillations) exhibit the same behavior as the experimental data. Therefore, our theoretical model satisfactorily describes the overall laser pulse chirp effect on the generated nanoacoustic strains for a broad range of chirp values.

In summary, we have investigated the role of the fs laser pulse chirp on the generated nanoacoustic strains in Ti:Si nanostructured materials. Using a sensitive transient reflectivity experimental technique, supported by an appropriately modified thermomechanical model, it was demonstrated that the laser-generated giant nanoscale acoustic strains can be controlled by altering the laser pulse chirp. Negatively chirped laser pulses induced higher amplitude strains inside Si than FTL and positively chirped laser pulses. Additionally, it was found that this behavior is non-monotonous giving rise to an optimum value for the laser chirp parameter to maximize the lattice strain effect. Thus, high resolution and fine tuning of the chirp parameter is required to further enhance the strain sensitivity. We showed that giant nanoacoustic strains in Si, a material of very high technological importance, can be all-optically controlled by at least a factor of two by altering the laser pulse chirp.

Acknowledgments

The authors would like to thank Prof. Panos Patsalas for the preparation of the samples and Dr. Giannis Orfanos for his valuable help on the data acquisition system. Authors also acknowledge support of this work by the project "ELI - LASERLAB Europe Synergy, HiPER & IPERION-CH.gr" (MIS 5002735) which is implemented under the Action "Reinforcement of the Research and Innovation Infrastructure", funded by the Operational Programme "Competitiveness, Entrepreneurship and Innovation" (NSRF 2014-2020) and co-financed by Greece and the European Union (European Regional Development Fund).

References

[1] B.C. Daly, G.A. Antonelli, H.J. Maris, W.K. Ford, L. Wong, E. Andideh, Measurements of the thermal conductivity of amorphous materials with low dielectric constants, Phys. B: Condens. Matter 316–317 (2002) 254–257.
[2] C. Rossignol, B. Perrin, B. Bonello, P. Djemia, P. Moch, H. Hurdequint, Elastic properties of ultrathin permalloy/alumina multilayer films using picosecond ultrasonics and Brillouin light scattering, Phys. Rev. B 70 (2004) 094102.
[3] N.-W. Pu, E.-Y. Pan, J. Bokor, Sensitive detection of laser damage to Mo/Si multilayers by picosecond ultrasonics, Appl. Phys. B 79 (2004) 107–112.
[4] S. Ramanathan, D.G. Cahill, High-resolution picosecond acoustic microscopy for non-invasive characterization of buried interfaces, J. Mater. Res. 21 (2006) 1204–1208.
[5] S. Kashiwada, O. Matsuda, J.J. Baumberg, R.L. Voti, O.B. Wright, In situ monitoring of the growth of ice films by laser picosecond acoustics, J. Appl. Phys. 100 (2006) 073506.
[6] T. Bienville, J.F. Robillard, L. Belliard, I. Roch-Jeune, A. Devos, B. Perrin, Individual and collective vibrational modes of nanostructures studied by picosecond ultrasonics, Ultrasonics 44 (2006) e1289–e1294.
[7] G.A. Antonelli, H.J. Maris, S.G. Malhotra, J.M.E. Harper, Picosecond ultrasonics study of the vibrational modes of a nanostructure, J. Appl. Phys. 91 (2002) 3261–3267.
[8] S.N. Jerebtsov, A.A. Kolomenskii, H. Liu, H. Zhang, Z. Ye, Z. Luo, W. Wu, G.G. Paulus, H.A. Schuessler, Laser-excited acoustic oscillations in silver and bismuth nanowires, Phys. Rev. B 76 (2007) 184301.
[9] T.C. Zhu, H.J. Maris, J. Tauc, Attenuation of longitudinal-acoustic phonons in amorphous SiO_2 at frequencies up to 440 GHz, Phys. Rev. B 44 (1991) 4281–4289.
[10] C.J. Morath, H.J. Maris, Phonon attenuation in amorphous solids studied by picosecond ultrasonics, Phys. Rev. B 54 (1996) 203–213.
[11] U. Storkel, K.L. Vodopyanov, W. Grill, GHz ultrasound wave packets in water generated by an Er laser, J. Phys. D: Appl. Phys. 31 (1998) 2258–2263.
[12] A.A. Maznev, D.J. McAuliffe, A.G. Doukas, K.A. Nelson, Wide-band acoustic spectroscopy of biological material based on a laser-induced grating technique, Ultrasound Med. Biol. 25 (1999) 601–607.
[13] H.J. Maris, Picosecond ultrasonics, Sci. Am. 278 (1998) 86–89.
[14] O. Matsuda, M.C. Larciprete, R.L. Voti, O.B. Wright, Fundamentals of picosecond laser ultrasonics, Ultrasonics 56 (2015) 3–20.
[15] C.B. Scruby, R.J. Dewhurst, D.A. Hutchins, S.B. Palmer, Quantitative studies of thermally generated elastic waves in laser-irradiated metals, J. Appl. Phys. 51 (1980) 6210–6216.
[16] J.D. Aussel, A. Le Brun, J.C. Baboux, Generating acoustic waves by laser: theoretical and experimental study of the emission source, Ultrasonics 26 (1988) 245–255.
[17] S.K. Sundaram, E. Mazur, Inducing and probing non-thermal transitions in semiconductors using femtosecond laser pulses, Nat. Mater. 1 (2002) 217–224.
[18] V.V. Temnov, C. Klieber, K.A. Nelson, T. Thomay, V. Knittel, A. Leitenstorfer, D. Makarov, M. Albrecht, R. Bratschitsch, Femtosecond nonlinear ultrasonics in gold probed with ultrashort surface plasmons, Nat. Commun. 4 (2013) 1468.
[19] N.-W. Pu, J. Bokor, Study of surface and bulk acoustic phonon excitations in superlattices using picosecond ultrasonics, Phys. Rev. Lett. 91 (2003) 076101.
[20] N. Stanton, R. Kini, A. Kent, M. Henini, D. Lehmann, Terahertz phonon optics in GaAs/AlAs superlattice structures, Phy. Rev. B 68 (2003) 113302.
[21] O. Matsuda, T. Tachizaki, T. Fukui, J.J. Baumberg, O.B. Wright, Acoustic phonon generation and detection in $GaAs/Al_{0.3}Ga_{0.7}As$ quantum wells with picosecond laser pulses, Phys. Rev. B 71 (2005) 115330.
[22] C.-T. Yu, K.-H. Lin, C.-L. Hsieh, C.-C. Pan, J.-I. Chyi, C.-K. Sun, Generation of frequency-tunable nanoacoustic waves by optical coherent control, Appl. Phys. Lett. 87 (2005) 093114.
[23] T. Shimada, C. Frischkorn, M. Wolf, T. Kampfrath, Maximizing the amplitude of coherent phonons with shaped laser pulses, J. Appl. Phys. 112 (2012) 113103.
[24] A.Q. Wu, X. Xu, Coupling of ultrafast laser energy to coherent phonons in bismuth, Appl. Phys. Lett. 90 (2007) 251111.
[25] C.M. Liebig, Y. Wang, X. Xu, Controlling phase change through ultrafast excitation of coherent phonons, Opt. Express 18 (2010) 20498–20504.
[26] O.V. Misochko, T. Dekorsy, S.V. Andreev, V.O. Kompanets, Yu.A. Matveets, A.G. Stepanov, S.V. Chekalin, Effect of intense chirped pulses on the coherent phonon generation in Te, Appl. Phys. Lett. 90 (2007) 071901.

[27] E. Tzianaki, M. Bakarezos, G.D. Tsibidis, Y. Orphanos, P.A. Loukakos, C. Kosmidis, P. Patsalas, M. Tatarakis, N.A. Papadogiannis, High acoustic strains in Si through ultrafast laser excitation of Ti thin-film transducers, Opt. Express 23 (2015) 17191–17204.
[28] E. Tzianaki, M. Bakarezos, G.D. Tsibidis, S. Petrakis, P.A. Loukakos, C. Kosmidis, M. Tatarakis, N.A. Papadogiannis, Controlling nanoscale acoustic strains in silicon using chirped femtosecond laser pulses, Appl. Phys. Lett. 108 (2016) 254102.
[29] J.-C. Diels, W. Rudolph, Ultrashort Laser Pulse Phenomena, Academic Press, San Diego, CA, 1996.
[30] B.C. Daly, K. Kang, D.G. Cahill, Attenuation of picosecond ultrasonic pulses in a thin silicon wafer, in: 1st International Symposium on Laser Ultrasonics: Science, Technology and Applications, Montreal, Canada, 16–18 July, 2008.
[31] H.N. Lin, R.J. Stoner, H.J. Maris, J. Tauc, Phonon attenuation and velocity measurements in transparent materials by picosecond acoustic interferometry, J. Appl. Phys. 69 (1991) 3816–3822.
[32] N.A. Papadogiannis, S.D. Moustaizis, Nonlinear enhancement of the efficiency of the second harmonic radiation produced by ultrashort laser pulses on a gold surface, Opt. Commun. 137 (1997) 174–180.
[33] N.A. Papadogiannis, P.A. Loukakos, S.D. Moustaizis, Observation of the inversion of second and third harmonic generation efficiencies on a gold surface in the femtosecond regime, Opt. Commun. 166 (1999) 133–139.
[34] C. Guo, G. Rodriguez, A.J. Taylor, Ultrafast dynamics of electron thermalization in Gold, Phys. Rev. Lett. 86 (2001) 1638–1641.
[35] S.I. Anisimov, B.L. Kapeliovich, T.L. Perel'man, Elektronnaya emissiya spoverkhnosti metallov pod deistviem ul'trakorotkikh lazernykh impul'sov, ZhETF 66 (1974) 776–779 [S.I. Anisimov, B.L. Kapeliovich, T.L. Perel'man, Electronemission from metal surfaces exposed to ultrashort laser pulses, Sov. Phys. JETP 39 (1974) 375–377].
[36] M. Lisowski, P.A. Loukakos, U. Bovensiepen, J. Stahler, C. Gahl, M. Wolf, Ultrafast dynamics of electron thermalization, cooling and transport effects in Ru (001), Appl. Phys. A 78 (2004) 165–176.
[37] B. Rethfeld, A. Kaiser, M. Vicanek, G. Simon, Ultrafast dynamics of nonequilibrium electrons in metals under femtosecond laser irradiation, Phys. Rev. B 65 (2002) 214303.
[38] E. Carpene, Ultrafast laser irradiation of metals: Beyond the two-temperature model, Phys. Rev. B 74 (2006) 024301.
[39] G.D. Tsibidis, Thermal response of double-layered metal films after ultrashort pulsed laser irradiation: The role of nonthermal electron dynamics, Appl. Phys. Lett. 104 (2014) 051603.
[40] C.K. Sun, F. Vallee, L.H. Acioli, E.P. Ippen, J.G. Fujimoto, Femtosecond-tunable measurement of electron thermalization in gold, Phys. Rev. B 50 (1994) 15337–15348.
[41] E.A.A. Pogna, S. Dal Conte, G. Soavi, V.G. Kravets, Y.-J. Kim, S. Longhi, A.N. Grigorenko, G. Cerullo, G. Della, Valle ultrafast spectroscopy of graphene-protected thin copper films, ACS Photonics 3 (2016) 1508–1516.
[42] G. Della Valle, M. Conforti, S. Longhi, G. Cerullo, D. Brida, Real-time optical mapping of the dynamics of nonthermal electrons in thin gold films, Phys. Rev. B 86 (2012) 155139.
[43] G. Della Valle, D. Polli, P. Biagioni, C. Martella, M.C. Giordano, M. Finazzi, S. Longhi, L. Duò, G. Cerullo, F. Buatier de Mongeot, Self-organized plasmonic metasurfaces for all-optical modulation, Phys. Rev. B 91 (2015) 235440.
[44] J. Garduno-Mejia, M.P. Higlett, S.R. Meech, Modelling the influence of nonthermal electron dynamics in thin and ultrathin gold films, Chem. Phys. 341 (2007) 276–284.
[45] J. Garduno-Mejía, M.P. Higlett, S.R. Meech, Morphology dependent ultrafast electron dynamics in ultrathin gold films, Surf. Sci. 602 (2008) 3125–3130.
[46] Z. Lin, L.V. Zhigilei, V. Celli, Electron-phonon coupling and electron heat capacity of metals under conditions of strong electron-phonon nonequilibrium, Phys. Rev. B 77 (2008) 075133.
[47] H. Teng, C. Guo, Chirp effects in femtosecond laser-induced surface second-harmonic generation from metals, Appl. Phys. Lett. 85 (2004) 1110–1112.